THE JOURNAL OF PHYSICAL CHEMISTRY B

ARTICLE

pubs.acs.org/JPCB

Magic-Angle Spinning NMR of a Class I Filamentous Bacteriophage Virus

Gili Abramov, Omry Morag, and Amir Goldbourt*

School of Chemistry, Raymond and Beverly Sackler Faculty of Exact Sciences, Tel Aviv University, Ramat Aviv 69978, Tel Aviv, Israel

Supporting Information

ABSTRACT: The fd bacteriophage is a filamentous virus that is widely used for bio- and nanotechnology applications ranging from phage display to battery materials. The possibility of obtaining a detailed description of its structural properties regardless of its state is therefore essential not only for understanding its physical arrangement and its bacterial infection process but also for many other applications. Here we present a study of the fd phage by magic-angle spinning solid-state NMR. While current structures rely on a Y21M mutant, experiments performed on a strain bearing a wild-type capsid report on high symmetry of the phage and lack of explicit subunit polymorphism. Chemical shift analysis confirmed that the coat protein mostly consists of a rigid right-handed curved α-helix (residues 6−47 of 50), preceded by a flexible loop-structured N-terminus. We were able to qualitatively assign the resonances belonging to the DNA, including the deoxyribose sugars and the thymine bases. These chemical shifts are consistent with base stacking and a C2′-endo/C3′-exo sugar pucker.

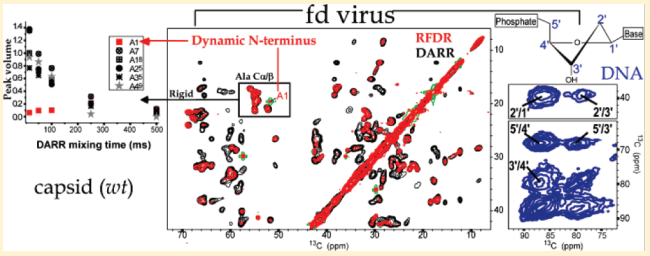

INTRODUCTION

The fd virion is a filamentous bacteriophage that infects strains of *Escherichia coli* bearing the F-pili.[1−3] Similarly to other inoviruses, it consists of a long circular right-handed single-stranded DNA that stretches to approximately 900 nm and is wrapped by thousands of small helical coat protein subunits.[4] Several different coat proteins cap the virion at both ends and participate in the assembly and infection processes. In recent decades, bacteriophages have been at the cutting edge of new developments in molecular biology, biophysics, and, more recently, bionanotechnology. Ff viruses (fd, M13, f1) have been extensively used for phage display technology,[5−8] as DNA and vaccine delivery vehicles,[9] and for the fabrication of nanomaterials.[10,11] The ease of genetic manipulation in Ff provides this diverse field of applications. Therefore, structural studies not only are important for understanding the structure and assembly of filamentous phage in general, but also can potentially provide a platform for characterizing the structural arrangement and properties in more complex phage-based materials.

The structures of a number of filamentous bacteriophages have been under study for many years now by X-ray fiber diffraction, NMR spectroscopy, cryo-EM, circular dichroism, and FTIR and Raman spectroscopies. The Pf1 phage, due to its rigidity, length (2 μm), and unique nucleotide-to-subunit ratio of unity, has been the paradigm virion for structural analysis. Its low-temperature structure has been refined several times by various experimental methods and refinement approaches.[12−15] Similar methods have been used to study the structure of fd. Initial studies showed that fd bearing a wild-type (wt) coat protein produces fanning of fiber diffraction layer lines,[16] prohibiting accurate structure determination. Similar studies using static solid-state NMR of aligned phage particles[17] showed severe line broadening, and in cryo-EM studies,[18] most of the wt particles did not converge to a common structure and the remaining data produced two different structures. In a different study, variability in protein−DNA interactions has been proposed as the source of polymorphism due to the noninteger nucleotide to subunit ratio, relying on the liquid crystalline properties of perturbed fd.[19] The experimental[20] ratio of 2.32 or theoretical[21] ratio of 2.4 between the number of DNA nucleotides and protein subunits causes nonuniform interactions between the DNA and capsid proteins in such a way that each nucleotide type potentially interacts with each of the four different positively charged lysine side chains in the C-terminus of the coat protein. Support for this distinction comes from mutation studies, in which replacement of one of these lysines (K48) with a noncharged residue resulted in extension of the phage, but replacement with arginine did not.[22] Another consequence of the noninteger ratio is the coiling of the virus particle with a persistence length of ∼3 μm for the wild type and ∼10 μm for the mutant, making Y21M essentially a rigid rod.[23]

High-resolution structures have therefore been developed based on the Y21M mutant.[18,24−26] The fd phage belongs to the class I family of inoviruses[27] having capsids with approximate C_5S_2 symmetry as distinct from the class II family with $C_1S_{5.4}$ symmetry.[28] Fiber diffraction data of highly ordered fibers

Received: May 3, 2011
Revised: June 23, 2011
Published: June 24, 2011

revealed that for all Ff bacteriophages, as in other class I phages, the 50-amino acid major coat protein subunits are arranged in pentamers that are related by a 2-fold screw axis with a rise of 16.15 Å. The exact C_5S_2 symmetry in fd is obtained when the Y21M coat protein mutant is used or when a low-pH sample is studied.[26] In other cases, as also predicted for other class I phages, the 2-fold axis is slightly perturbed and pentamers are related by a rotation of 182.70° and a rise of 16.0 Å.

The helical nature of the coat protein subunit has been deduced in very early studies;[29,30] however, the extent of helicity varies between models due to the ill-defined unstructured N-terminus that did not produce proper electron density in diffraction studies or cryo-EM. Recent structures used mutual refinement of solid-state NMR and fiber diffraction data,[24] and the differences from other structures have also been discussed in detail.[31] Early studies of protein dynamics revealed that, in addition to N-terminus dynamics, the aromatic rings undergo fast ring flips but the backbone is rigid.[32,33] The DNA structure in fd has been investigated by a variety of electronic and vibrational spectroscopies as well as static solid-state NMR. The DNA backbone has been reported to be right-handed with stacked bases and highly disordered.[34−38] ^{31}P NMR of static aligned fd phages have been inconclusive and showed that despite proper alignment of the sugar rings and protein subunits, the OPO bond angles show a distribution of orientations.[35] Results from Raman studies support this observation.[37] Raman bands typical of both C2′-endo and C3′-endo sugar pucker conformations have been observed in several studies.[36−38] Ultraviolet Raman resonance (UVRR) studies showed that the dG markers are indicative of a C3′-endo/anti conformation rather than a C2′-endo/anti conformation.[38] In addition, the large hypochromism in fd was associated with strong base stacking, in large contrast to Pf1.[39,40]

We have shown recently that magic-angle spinning (MAS) solid-state NMR can be used to study an intact bacteriophage[41−43] and provide comprehensive information on a single sample that complements many different methods. The application of MAS NMR to the Pf1 phage provided insight into its structure and dynamics and into the effect of its structural phase transition on intersubunit packing. In this study we use MAS NMR to study the intact and fully hydrated class I fd phage. We demonstrate that narrow and well-resolved lines are achievable for a strain bearing a wild-type coat protein and on the basis of almost complete assignment of the coat protein resonances many chemical-shift-based structural properties can be derived. Our data indicate that a single conformation of the *wild-type* coat protein subunit exists throughout the virion's capsid; the coat protein itself has a mobile N-terminus connected to a helical stretch spanning residues 6−47 (or 48). We also observe clear signatures of the deoxyribose sugar and thymine resonances indicative of the DNA structure.

EXPERIMENTAL METHODS

Phage and Host Constructs. The fd phage we use (fth1 vector; obtained from Prof. Gershoni) is a constructed hybrid phage containing the genome of wild-type fd and two insertion positions in its genome, a segment of transposon Tn*10* coding for tetracycline antibiotic resistance (*tetA* segment) and another segment, *pVIIISTSh*, a gene that can incorporate a mutated coat protein for the purpose of phage display, attached between the *pIII* and *pVII* genes.[44] The hybrid phage infects male strains of *E. coli* bearing incompatibility group F (*incF*) elements, thereby transducing the infected cells to tetracycline resistance. The fth1 strain is genetically stable and produces high titers of recombinant phage. This construct has ∼3430 subunits that are identical to the wild-type fd (∼2700 subunits). We used the DH5α strains of *E. coli* (obtained from Prof. Benhar) for phage production.

Preparation and Purification of fd Phage. A single colony of the host was initially grown in a rich medium to log phase (∼10^8 cfu/mL; OD_{600} (optical density at 600 nm) = 0.6) and then infected with the phage in a multiplicity of ∼10. An aliquot of the infected culture (at a ratio of 1/100) was transferred to a minimal nutrient medium (M9) having $^{15}NH_4Cl$ and [^{13}C]glucose as the sole sources of nitrogen and carbon (both >99% enrichment, obtained from Cambridge Isotope Laboratories). Rapid shaking (240 rpm) and aeration for ∼24 h yielded phage titers of >10^{12} pfu/mL. Bacteria were pelleted at 8000 rpm, and the phage in the supernatant solution was isolated and precipitated with 5% (w/v) polyethylene glycol (PEG) 8000 (ABCR GmbH & Co. KG) and 0.5 M NaCl. The PEG precipitated phage was spun down at 8000 rpm for 45 min and resuspended in 10 mM Tris buffer, pH 8.0. The clarified fd phage solutions were brought to a density of ∼1.31−1.32 g/cm^3 with CsCl (Chem-Impex International) and centrifuged to equilibrium at 37 000 rpm for 51 h (4 °C) in Beckman SW41 rotors. The viscous central band of the virus in the middle of the tube was carefully separated by a pipet from the upper and lower bands. The solution of recovered virus was diluted to ∼1 mg/mL, PEG-precipitated, and resuspended in the Tris buffer, thereby eliminating the high Cs^+ concentration. A sample containing high Cs^+ content was also studied. The virus had a UV absorbance spectrum with a maximum at 269 nm, a minimum at 245 nm, and an OD_{269}/OD_{245} ratio of 1.36. The concentration of phage particles was calculated on the basis of the specific absorbance coefficient at wavelength maxima, which is 3.84 A mg^{-1} mL for fd.[19] Spectra from two different sample preparations are shown (see the Results).

NMR Sample Preparation. Purified virus solutions at ∼1 mg/mL were made 5% (w/v) in PEG 8000. Upon the addition of 5 mM $MgCl_2$, the virus was quantitatively precipitated. Samples were transferred by centrifugation (at 14 000 rpm) to a 4 mm ZrO_2 rotor via several intermediate transfer steps using sealed tips, yielding fully hydrated fd samples of 7−16 mg in a volume of approximately 30−50 μL. The two samples were spun for different times after precipitation and therefore resulted in different densities. The virus was recovered after NMR data collection and found to have preserved its infectivity.

NMR Experiments. All MAS solid-state NMR experiments were acquired on a Bruker Avance-III spectrometer operating at a static magnetic field of 14.1 T, corresponding to Larmor frequencies of 600.2 MHz for ^{1}H, 150.9 MHz for ^{13}C, and 60.8 MHz for ^{15}N. Experiments were performed using a 4 mm wide-bore (WB) triple-resonance probe operating at H−C−N frequencies using MAS rates of $\omega_r/2\pi$ = 12−13.5 kHz and a temperature set between −15 and +3 °C on the controller. Spinning at 12 kHz added approximately 10−15 deg due to friction. ^{13}C chemical shifts were referenced externally using the adamantane sample as a secondary reference, assuming a chemical shift of 40.48 ppm for the CH_2 carbon line;[45] ^{15}N shifts were externally referenced using solid $^{15}NH_4Cl$ (39.27 ppm with respect to liquid ammonia at 25 °C[46]). Site-specific assignments were obtained by performing two-dimensional (2D) and three-dimensional (3D) experiments. More specifically, we acquire data using 2D DARR (dipolar assisted rotational resonance[47,48]), 2D RFDR (radio frequency driven recoupling[49]), and intraresidue

NCACX and sequential NCOCX experiments[50−55] using DARR mixing.

2D DARR and RFDR experiments used 1.2−3 ms $^{1}H-^{13}C$ linearly ramped (10%) cross-polarization[56−58] (CP), with the center of the ramp corresponding to the first Hartmann−Hahn spinning sideband, i.e., $\omega_{1H} = \omega_{1C} + n\omega_R$ ($\omega_{1x} = -\gamma_x B_1$, irradiation strength on nucleus x, $\omega_{1H} = 65$ kHz). For proton decoupling at 70−80 kHz, the two-pulse phase modulation[59] (TPPM) and the swf-tppm[60] schemes were used. DARR spectra were acquired with mixing times of 15−500 ms and RFDR spectra with a mixing time of 3 ms. The ^{13}C frequency was centered around 107 ppm (±7), and for all pulses, $\omega_{1C} = 50$ kHz. The 2D data sets were acquired using 1024 and 4096 points and acquisition times of 12.8 and 20.5 ms for t_1 and t_2, respectively; each FID was a sum of 16 or 32 scans using a recycle delay of 2.7 s (5 times the T_1 relaxation time of protons, determined by a saturation recovery experiment), yielding a total experimental time of 13−24 h for each 2D experiment.

For the 3D N−C−C experiments $^{15}N-^{13}C$ magnetization transfer was achieved using a band-selective tangential CP.[59,61,62] for NCACX $\omega_{1N} = 2.5\omega_r$ and $\omega_{1C} = 1.5\omega_r$; opposite conditions were used for NCOCX. All 3D experiments were acquired using a minimal acquisition time of 10 ms in the indirect dimensions and 25 ms in the direct dimension. Explicit values are given in the Supporting Information; 16 scans were acquired using a recycle delay of 2.7 s, yielding a total experimental time of ∼5 days for the NCACX experiment and ∼3 days for NCOCX.

Data Analysis. All NMR data were processed using Topspin2.1 and NMRPipe.[63] Analysis was performed using SPARKY,[64] version 3.114, and NMRDraw.[63]

RESULTS

Resonance Assignment: Coat Protein. Procedures and techniques for assignment of solid-state NMR data have been described and applied in many different systems such as globular proteins,[65−74] membrane proteins,[75−79] amyloids,[80−84] etc. ^{13}C and ^{15}N site-specific resonance assignment of the major coat protein atoms in the fd virion were carried out through the analysis of 2D homonuclear $^{13}C-^{13}C$ correlation and 3D heteronuclear $^{15}N-^{13}C-^{13}C$ correlation experiments, all conducted on uniformly ^{13}C and ^{15}N labeled intact virus particles.

A characteristic 2D $^{13}C-^{13}C$ DARR spectrum of fd, shown in Figure 1, features cross-peaks stemming from the ∼3430 coat protein subunits, which constitute ∼83% of the virion mass (approximately 22 MDa for the fully labeled particle). The DNA (14% in weight) signals resonate mostly at chemical shifts different from those of amino acids. These signals were also detected in our spectra, as will be detailed later on. Minor coat proteins (gp3, gp6, gp7, gp9) comprise up to 3% of the total mass[85] and are undetectable.

To facilitate the assignment process, we initially identified the various spin systems for amino acids with well-isolated chemical shifts such as the Cα/Cβ signals of Ala, Ser, Asp, and Thr, the side chain patterns of Ile and Val, and the backbone carbons of Gly. The unique shifts of the isoleucine side chain residues and the single proline residue in position 6 are indicated in Figure 1, as well as the site-specific assignments of many other amino acids. Those assignments were obtained by detecting inter-residue $C\alpha(i)-C\alpha(i \pm 1)$, $C\alpha(i)-C\beta(i \pm 1)$, and $C\beta(i)-C\beta(i \pm 1)$ interactions using longer mixing times in the DARR experiment and by combining nitrogen shifts from the 3D experiments. An overlay of DARR spectra with mixing times of 100 ms (blue) and 15 ms (green) is shown in Figure 2, demonstrating the assignment of many homonuclear inter-residue peaks. The intense and well-isolated inter-residue cross-peaks associated with glycine residues have been essential for initiating the assignment process, but many other resonances have been clearly resolved as well.

Identification of all amino acids was not possible using only the DARR experiment, and especially those residues that are thought to exhibit increased dynamics in the N-terminal part of the protein were missing (A1, E2, G3) or very weak (D4) in the short mixing time experiments. These residues could be readily indentified using the 2D RFDR experiment, Figure 3. The RFDR spectrum exhibits a reduced number of peaks due to band selectivity and a short mixing time; however, the N-terminal residues exhibit intense and narrow J-split resonances. These peaks can be easily linked to A1, E2, and G3 using their database average chemical shifts and are consistent with a nonhelical region.[86,87] These N-terminal residues could be weakly detected also at long mixing times of the DARR experiment or using the more condensed sample at lower temperatures. At these conditions, the dynamic methyl group of Met28 could also be detected (100 ms DARR, −5 and −15 °C). The reduction in temperature or change of sample did not produce apparent shift perturbations of values larger than 0.2 ppm.

Further site-specific assignments, and shifts for nitrogen resonances, were obtained using 3D experiments. Following regular procedures for the assignment of solid-state NMR data,[52,65,68] the unique high-field ^{15}N shifts of glycines, serines, and threonines could be easily identified, linked to neighboring backbone carbons, and used as starting points for the sequential assignment process. Strip plots (for residues 15−21) supporting our data assignment are shown in Figure 4. The high α-helical nature of the coat protein caused overlap even in the 3D spectra, especially in the hydrophobic region, where a repetitive sequence such as ^{29}VVVI^{33}V hinders clear distinction of backbone resonances. Of the four valines, V33 could be linked to G34 and specifically assigned, a cross-peak V31−I32 was identified in the low-temperatures dense-sample conditions, and the remaining V29 and V30 were ambiguously assigned (a single full side chain pattern was identified that belongs to one of these valines). Another complex region which lacked resolution was the DNA interaction region (40−48) and especially the lysine residues. The only lysine in the amphiphatic region (Lys8) could be easily linked to its adjacent Ala7 and Ala9 by virtue of their distinct Cβ shifts (19.3 and 18.0 ppm). Lysines at positions 43 and 44 are both attached to Phe residues (^{42}F^{43}K^{44}K^{45}F) that share a similar Cα shift but different Cβ shifts (39.9 and 37.9). Correlations of Lys Cα and Cγ with the different Phe Cβ carbons in the 2D experiments allowed the distinction between those lysines. Lys40 was identified by observing a cross-peak between its Cβ carbon and the Cβ and Cδ1 carbons of Ile39 in the long mixing time DARR experiment, and Lys48 remained unassigned due to strong peak overlap.

Aromatic Residues. The assignment of aromatic residues is many times hindered by internal dynamics, spectral congestion, and broadening by scalar couplings in the case of fully labeled samples. The role of the aromatic residues in understanding the structure, dynamics, and intersubunit packing in the fd phage, and the ability to compare their properties to studies by other spectroscopic methods,[32,88−90] renders their assignment essential for further structural studies. In the case of fd, the complete assignment of the tryptophan-26 and tyrosine-21 and -24 side

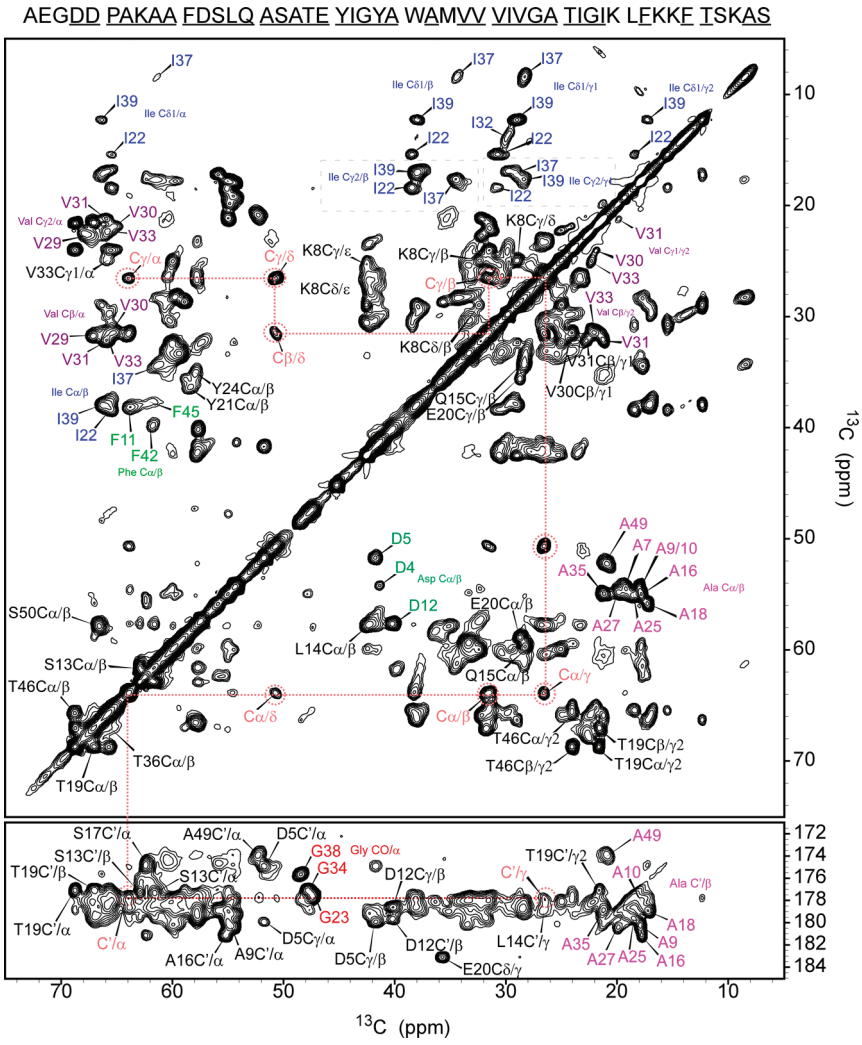

Figure 1. 2D $^{13}C-^{13}C$ DARR spectrum of the fd virion showing intraresidue cross-peaks. The explicit assignments noted in the spectrum are underlined in the amino acid sequence of the coat protein shown on top. The complete amino acid pattern of the single proline residue in position 6 is marked with a dotted red line. Data were acquired on a 600 MHz spectrometer using a 15 ms mixing time and a set temperature of −5 °C. The spectrum was generated by a Lorentz-to-Gauss transformation in both dimensions. Fifteen contours at multiples of 1.4 were generated starting at a signal-to-noise ratio of 10 for the aliphatic region and 13 for the carbonyl region.

chain rings has been facilitated by using the more condensed sample and long mixing times. Verification of side chain resonances was obtained using many inter-residue contacts, for example, Tyr21 to Glu20 and Ile22 and Tyr24/Trp26 to Ala25. The complete pattern for these residues has been observed and is shown in Figure 5. The Tyr21 amino acid, which was normally mutated for other studies, shows well-resolved lines and no apparent polymorphism, as do Tyr24 and Trp26. Phenylalanine identification was obtained by detection of the residue types in short mixing time experiments (15 ms, DARR, Cα−Cγ), linkage to neighboring amino acids in 3D and long mixing time 2D experiments (A10−F11−D12, F45−T46), and elimination (F42).

DNA Signals. Cross-peaks from DNA sugars and the thymine base were clearly resolved in our spectra and are shown in Figure 6. A sum projection of the presented spectral region shows the approximate line widths of the various sugar resonances. The deoxyribose sugar signals could be observed in almost every spectrum; however, the most intense and broad lines could be clearly assigned in the more condensed sample. The different carbon resonances were assigned qualitatively following their average database values and their spatial proximity. The following average shifts (ppm) and line widths (Hz) have been obtained: C1′, 86.2 (740 Hz); C2′, 39.9 (750 Hz); C3′, 79.9 (620 Hz); C4′, 86.8 (660 Hz); C5′, 68.2 (370 Hz). For the thymine bases, chemical shifts were obtained by the appearance of cross-peaks with the unique methyl group at 14.5 ppm, and their values are as follows: C2, 153.8 (200 Hz); C4, 168.8 (320 Hz); C5, 113.8 (380 Hz); C6, 138.9 (410 Hz); C7, 14.5 (240 Hz).

DISCUSSION

Assignment, Conformation, and Dynamics. Resonance assignments have been achieved using a combination of the data from short and long mixing time 2D homonuclear experiments, in conjunction with well-resolved 3D data. Similarly to Pf1,[41] assignment of the amphiphatic part could be easily and quickly obtained due to the variability and type of amino acids and the rigidity of the coat protein. This is demonstrated clearly in the strip plots (Figure 4) and Cα−Cα region of the long mixing time

dx.doi.org/10.1021/jp2040955 |J. Phys. Chem. B 2011, 115, 9671–9680

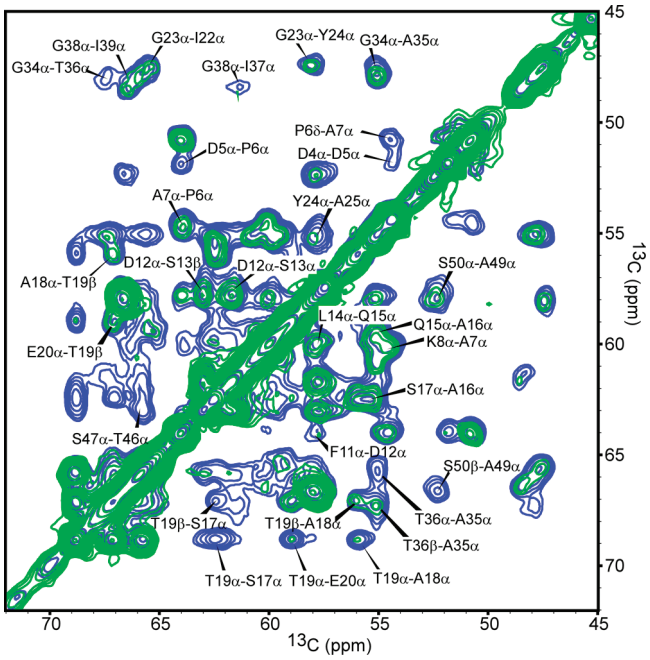

Figure 2. 2D $^{13}C-^{13}C$ DARR spectra of fd recorded with 100 ms (blue) and 15 ms (green) mixing times. The region shown above contains mainly inter-residue Cα−Cα and Cβ−Cα correlations, as indicated. Such correlations facilitated the site-specific assignment process. Spectral details are similar to those of Figure 1.

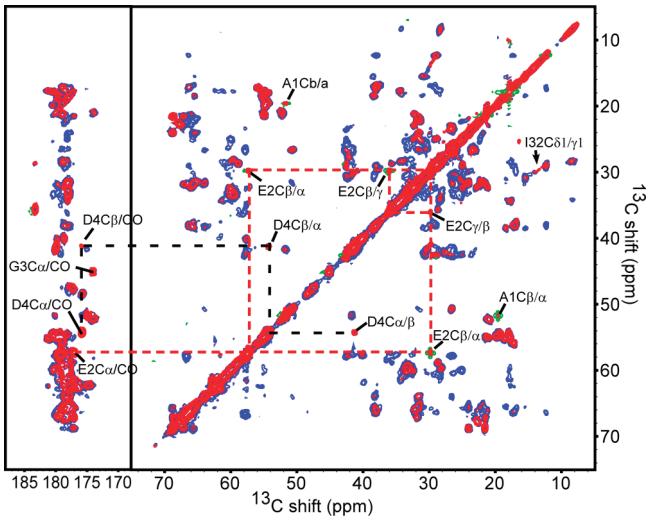

Figure 3. Overlay of RFDR (3 ms, red) and DARR (15 ms, blue) spectra of the fd phage. The spin systems for the N-terminal amino acids A1, E2, G3, and D4 are noted and indicated by the dashed lines. Both spectra were taken at the same temperature and processed with a Lorentz-to-Gauss window function in both directions. The terminal amino acids exhibit very narrow lines with line widths of 75 Hz on average.

DARR experiments (Figure 2). The usability of the Cα−Cα inter-residue contacts has already been demonstrated for such symmetric and high molecular weight proteins as the type III secretion system PrgI needle protein.[92] Overall, we have obtained a sufficient amount of data to probe the conformation of the protein subunit within the intact phage and obtain a qualitative view of the protein dynamics. The prediction of torsion angles using TALOS+[93] and PREDITOR[94] shown in Figure 7, results from probability-based secondary structure prediction,[87] and the sign of $\Delta C\alpha - \Delta C\beta$[95] (positive for a helix), all show that the coat protein subunit is mostly a right-handed α-helix starting at Pro6 and ending at Ser47 or Lys48. Since approximately 5% of proline residues may adopt a cis peptide bond conformation,[96] we used the difference between its Cβ and Cγ shifts (<8 ppm) to determine that it is in a trans configuration,[97] in agreement with all other Protein Data Bank (PDB) structures of fd. A comparison of the ϕ and ψ values predicted from NMR shifts with those of PDB entries 2C0X and 2C0W[24] and 1NH4[25] indicates some smoothing of the secondary structure in the helical region, probably since the protocol is based on trios of residues to obtain dihedral angles. Nevertheless, slight bending of the helix is reproduced, and the N-terminus shows a clear nonhelical orientation. On average (residues 6−47), for the NMR−TALOS+ prediction $\phi = -64.2 \pm 2.7°$ and $\psi = -41.1 \pm 3.1°$, while for 2C0W a much larger variability is observed ($\phi = -67.2 \pm 12.4°$ and $\psi = -37.1 \pm 13.2°$), and similar trends hold for 2C0X and to a lower extent also for 1NH4 (standard deviation of 6−7°). In all cases the deviations from the ideal straight helix ($\phi = -57°$, $\psi = -47°$) are in agreement with a slight curvature. Curved helices appear regularly in protein structures, and a survey of over 1000 short helices (9−37 residues) showed that the mean values are $\phi = -63 \pm 7°$ and $\psi = -43 \pm 8°$, much closer to the values obtained for fd. We also compared the first side chain torsion angle χ_1 (N−Cα−Cβ−Cγ) that is predicted by PREDITOR to those of PDB entry 2C0X. We find that agreement between the fiber diffraction and chemical-shift-based predictions exists for residues 6−22 (with the exception of F11; Ala and Gly lack a χ_1 angle), which have all been assigned to a gauche+ (g+) conformation; alternating g+ and trans conformations have been predicted by both methods for residues 28−39, and residues 46−47 are in g+ conformation in both cases. Interestingly, the only significant differences (with the exception of residues 24 and 26) lie within the DNA interaction domain (K40−F45), where the fiber diffraction data suggest for all χ_1 angles a g+ conformation, while NMR−PREDITOR suggests an all-trans conformation, albeit with moderate confidence values (0.5−0.8).

In the N-terminus, the NMR-predicted torsion angles are consistent with a nonhelical region, similarly to the reported results on the Y21M mutant.[25] The torsion angles for residues E2 and G3 (TALOS, $\phi_2/\psi_2 = -57 \pm 42°/132 \pm 10°$, $\phi_3/\psi_3 = 92 \pm 15°/-8 \pm 17°$) are consistent with a type II turn[98] (also predicted from submitting these angles to DSSP calculations[99]). These results are in good agreement with the structures mentioned above (with the exception of ψ_5, which has a value of $\sim 180 - \psi_{NMR}$). In an early study by static solid-state NMR of the fd bacteriophage,[33] it was proposed that Ala, Gly, and Asp (associated with residues 1, 3, and 4) in the N-terminus are motionally averaged on the millisecond time scale. In cryo-EM studies, no electron density was observed in this region, and in X-ray studies the electron density in this region was ill-defined.[24] Our NMR data provide supportive evidence for the flexibility of this region; the appearance of the resonances associated with this region only at long mixing times and the slow DARR buildup curves (Figure 8) relative to other single-bond cross-peaks of the same amino acid types suggest time averaging of the dipolar interaction. The increased dynamics is also apparent in the narrow resonances observed in the RFDR spectra (Figure 3).

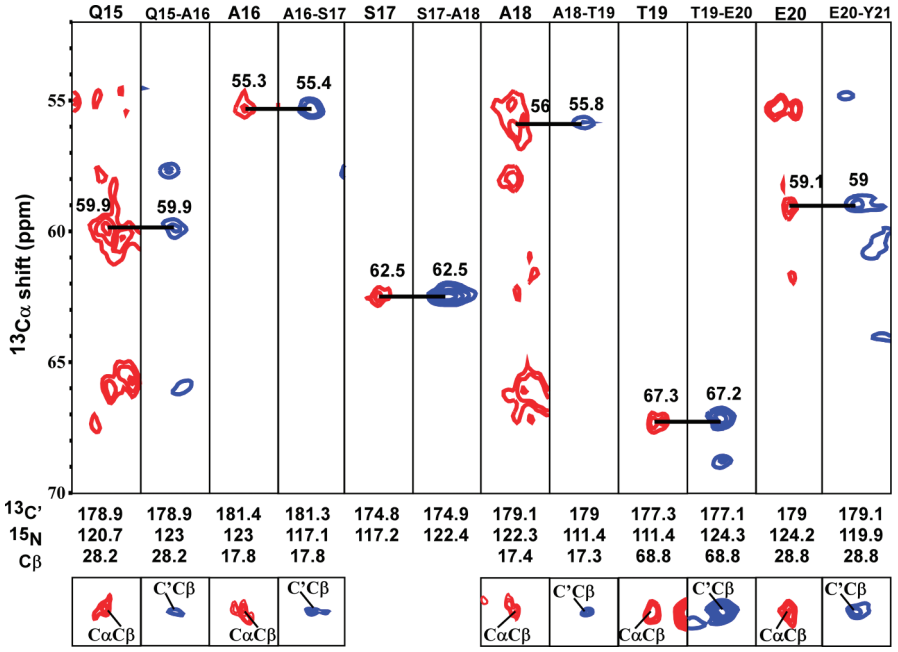

Figure 4. Strip plots from 3D heteronuclear correlation experiments for residues 15−21 of the fd capsid. Red and blue spectra correspond to intraresidue NCACX and sequential NCOCX experiments, respectively. ^{15}N shifts and the center of the carbonyl (C′) axis (width 2.5 ppm) corresponding to the particular strip are indicated at the bottom of the strip. Horizontal bars link the strips from ^{15}N planes of residues i and $i-1$ that share the C′−Cα peaks of residue $i-1$. The bottom subspectra correspond to 2D planes at the same ^{15}N shift and display N−C′−Cβ or N−Cα−Cβ cross-peaks; the vertical axis is centered on either Cα or C′. Both spectra were processed with a shifted sine bell in the carbon dimensions and exponential broadening (20 Hz) in the ^{15}N dimension.

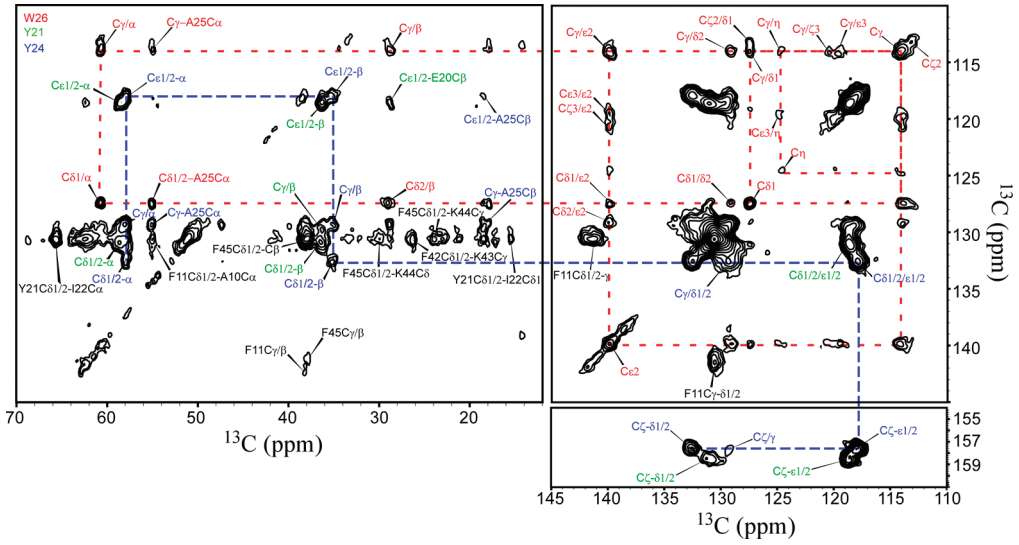

Figure 5. Aromatic region of a 2D $^{13}C-^{13}C$ DARR (15 ms) spectrum. Full amino acid patterns for Trp26, Tyr21, and Tyr24 are indicated, along with several inter-residue correlations. The spectrum was processed with a Lorentz-to-Gauss transformation.

Lack of Global Polymorphism in fd. The fd phage, much like Pf1, has been studied extensively by various spectroscopic tools, as it is a paradigm structure for a class I bacteriophage. Nonetheless, structural studies using fiber diffraction, static solid-state NMR, and cryo-EM all report an inhomogeneous structure of the wild-type coat protein. X-ray results for the wild-type phage report "layer-line fanning" (fiber diffraction), which is eliminated either by reducing the pH below the isoelectric point (pH 4.0) or by using a Y21M mutant.[16] These observations were explained by the tilting of the virions from the alignment axis and by the charge distribution and intersubunit hydrogen bonding. In static solid-state NMR spectra, conformational heterogeneity was manifested in significant spectral line broadening of the wild-type phage;[17] however, for the Y21M mutant individual resonances were observed, allowing the derivation of a high-resolution backbone structure.[25] Results from electron microscopy reported the existence of two different converging structures in the mutant and an additional large group of nonconverging

dx.doi.org/10.1021/jp2040955 |J. Phys. Chem. B 2011, 115, 9671–9680

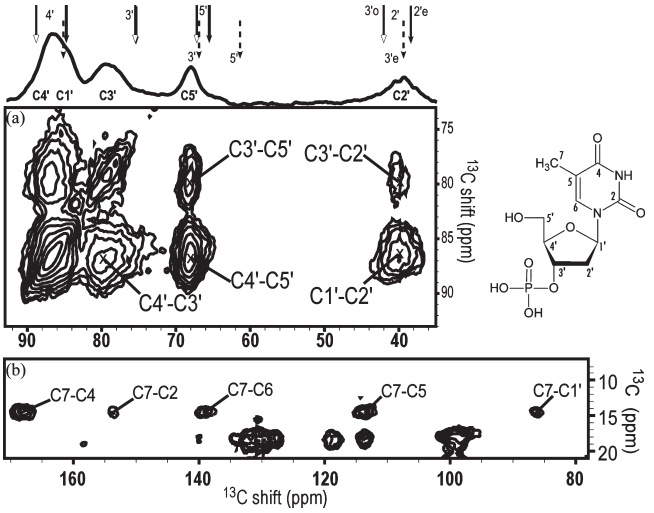

Figure 6. Qualitative assignment of DNA signals from the DARR experiment (100 ms at −5 °C), processed with exponential line broadening of 80 Hz. (a) Signals of the deoxyribose sugar and the sum-projection spectrum. Average chemical shifts of 2′-endo (solid arrows), 3′-exo (solid lines, empty arrows), and 3′-endo (dash arrows) from Santos et al.[91] are indicated, suggesting a sugar pucker closer to 2′-endo or 3′-exo (see the Discussion). (b) Thymine cross-peaks within the pyrimidine base and the C7−C1′ cross-peak to the deoxyribose. Notations for the nucleotide and deoxyribose are noted on the molecule.

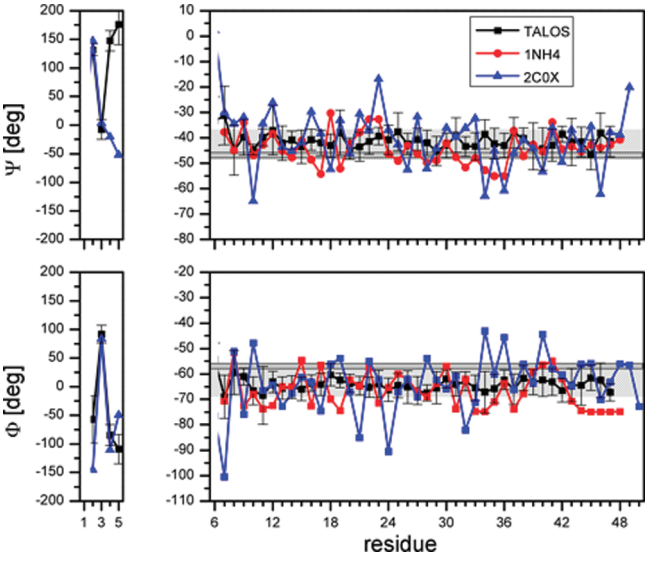

Figure 7. Chemical-shift-based predictions of the torsion angles ϕ and ψ for the fd coat protein (black) using TALOS+. The NMR data are compared to those of two previously proposed structures, 2C0X (blue) and 1NH4 (red). Residues 1−5 are drawn on a different scale and according to the predicted angles correspond to a nonhelical region, probably a turn. Residues 6−47 suggest a continuous helical conformation. In all cases, the structure slightly deviates from an idealized straight helix (gray area at $\psi = -47 \pm 1°$ and $\phi = -57 \pm 1°$) and manifests the expected curved helical structure of the coat protein (slanted area at $\psi = -43 \pm 6°$ and $\phi = -63 \pm 6°$).

structures for the wild type.[18] Moreover, it was suggested that heterogeneity exists within a single virion particle. In a somewhat different view, the polymorphism in the fd phage was attributed to the nonequivalence of subunits and nucleotides forcing

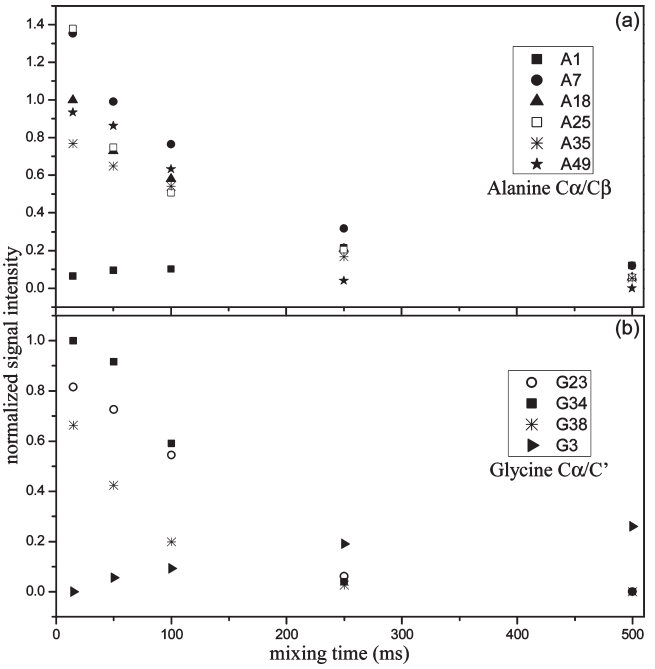

Figure 8. Single-bond DARR buildup curves for Ala and Gly residues in fd. Data points were obtained by integration of the 2D cross-peak volumes using the Gaussian line shape fitting routine in SPARKY. The signals were normalized according to the volume of (a) A18 and (b) G34.

different subunits to interact with different nucleic acid bases.[19]

In view of these observations, it is interesting that our studies on a fully hydrated fd phage bearing a wild-type coat protein do not report any subunit polymorphism; the excellent resolution clearly demonstrates single peaks for resonances belonging to all the atoms we could assign in the coat protein, and we could not allocate any evidence for peak splitting arising from site-specific polymorphism. Examples for the homogeneity of the coat protein are many; the complete side chain pattern of proline reports single resonances for all its carbons (Figure 1); the isoleucine side chain resonances of Ile22, Ile39, and Ile37 are well resolved and show single resonances; residues that are highly congested can be resolved by virtue of inter-residue contacts, and these cross-peaks together with other inter-residue side chain contacts also report a single conformation of the subunit. Finally, full pattern recognition of the Trp and Tyr aromatic residues (Figure 5) also indicates the existence of a single conformation of those amino acids, which have been reported to be involved in intersubunit packing.

The only residue that exhibits some conformational heterogeneity is Ile32. At all conditions, including the RFDR experiment, the side chain Cδ and Cγ1 atoms show broad and dispersed signals. It is not clear why only Ile32 shows these features repeatedly in all samples and at all conditions we used, and whether it is related to the fact that mostly mutagenesis of this amino acid has failed.[26] Ile32 may play a role in intersubunit packing; however, in current models it points inward toward the DNA and does not interact closely with neighboring subunits. It is possible that the variability in the DNA structure affects Ile32 due to its long side chain pointing inward; however, this assumption needs to be further validated.

Our data indicate that the Y21M mutant probably allows better interviral packing and alignment rather than an actual modification of the subunit conformation, which is homogeneous for the wt capsid. This observation is in agreement with recent measurements of the persistence length of the wild-type fd that was shown to be much shorter than that of the mutant[23] (2.8 ± 0.7 μm for wt vs 9.9 ± 1.6 μm for Y21M). According to the NMR data, it is highly unlikely that subunit polymorphism exists, not between different virus particles, and not within the same virion. Any polymorphism affecting the large length scale coiling must be manifested in the variability of subunit−DNA interactions, which seem to have a negligible effect on the subunit structure and dynamics and on the NMR data (with the possible exception of Ile32).

DNA in the fd Bacteriophage. Current studies of the DNA in fd report that the phosphodiester backbone is disordered and mobile. These observations were based on the unmodified and broad static solid-state NMR spectrum of aligned fd[35] and the lack of typical Raman markers of A-form and B-form DNA.[37] This fact does not contradict the observations of ordered sugars and bases. Raman hypochromism suggests dense stacking of the bases[38,39] in fd, and markers for deoxythymidine (dT) and deoxyguanosine (dG) bases indicate both C3′-endo/anti and C2′-endo/anti sugar puckers. While dG bases are clearly in the C3′-endo/anti conformation[36−38] (which switches to C2′-endo/anti in the free fd-extracted DNA), markers for dT report a significant amount of these bases in a C2′-endo conformation. dA and dC markers in these studies have been inconclusive.

As reported in the Results, we could clearly identify signals arising from the deoxyribose sugars and from dT, which constitute approximately 34% of all bases in fd.[100] While site-specific assignment of sugars to the sequence position or even to the attached bases (with the single exception of dT/C1′−dT/C7) is impossible at this stage due to a lack of resolution or sufficient signal-to-noise ratio, their chemical shifts can report the sugar pucker. Several studies tried to establish a correlation between the sugar pucker and the carbon chemical shifts.[91,101−103] Most sensitive to such conformational changes are the C3′ and C5′ carbons, shifting approximately 8 ppm downfield on going from C3′-endo to C2′-endo or C3′-exo. C4′ and C5′ show the same trend, with C5′ shifting between 4 (2′-endo) and 6 (3′-exo) ppm on average.[91] Considering all resonance values assigned to fd DNA, and especially the low-field shifts of C3′, C4′, and C5′, our data are more consistent with the C2′-endo/C3′-exo conformations. This can also be seen visually in Figure 6, where the chemical shift positions of the three ribose conformations are indicated on top of the sum spectrum. The C3′ resonance is very broad, yet it is far from the regime assigned to C3′-endo. Additionally C5′, which exhibits the narrowest line width (<400 Hz), is clearly in the C3′-exo range, and no signal is detected at all in the expected region of C3′-endo (61 ppm). In view of the clear C3′-endo Raman markers for dG, this is a surprising result and may indicate large variability in the structure of the DNA in fd. It may also be a manifestation of the different sample conditions; however, the chemical shifts we observed are reproduced in different sample concentrations, temperatures, and ionic strengths (we detect a deoxyribose signal in a Cs-rich sample at similar chemical shifts). Another interesting observation is in comparison to Pf1. The Pf1 DNA chemical shifts for all bases and sugars have been observed by using a combination of DNA-labeling techniques, low-and high-field studies, and dynamic nuclear polarization NMR.[104] Interestingly, while the stacking properties and backbone conformations of fd and Pf1 are completely different,[15,35,36,40,100,105] and are manifested here in the different dT resonances of C4, C5, and C7, there seem to be large similarities between their sugar puckers when considering the sugar chemical shifts.

CONCLUSIONS

The 22 MDa fd bacteriophage, a class I virion, has been studied by magic-angle spinning solid-state NMR. The complete list of assignments appears in the Supporting Information and has been deposited in the Biological Magnetic Resonance Bank.[106] The data acquired on an intact fully hydrated sample show that the 3430 wild-type coat protein subunits possess a single conformation, which is made of a rigid α-helix stretching over residues 6−47/48 and a mobile N-terminus with a loop structure. No polymorphism was evident from our experiments (with the possible exception of the side chain of Ile32), and the short persistence length of the wt phage does not seem to affect or degrade the MAS NMR data. Many of our observations have been based on chemical shift analysis, which has become an increasingly important marker for structure.[107,108] While for protein structure these methods are well established, they are still in developmental stages for DNA and RNA studies, and even more so for the study of protein−DNA interactions. Nevertheless, the C3′ and C5′ shifts clearly indicate an S-type sugar pucker (different from Raman studies), and the thymine base shifts are consistent with base stacking, in agreement with the current literature. In summary, MAS NMR allows us to study the structure and dynamics in intact wild-type filamentous phage belonging to class I symmetry, regardless of its coiling properties. Also, it provides unique information on the side chains and possible intersubunit interactions, which are otherwise less amenable to other types of spectroscopies. The fd phage is a paradigm structure for many other phages, and a biomaterial that is used for many applications ranging from phage display to nanomaterials; our study therefore opens routes to characterize such systems in detail, regardless of their shape and form.

ASSOCIATED CONTENT

Supporting Information. Full list of chemical shifts, experimental and processing parameters, comparison of the backbone χ_1 torsion angle from NMR predictions to those of PDB entry 2C0X, comparison of TALOS+ and PREDITOR ϕ and ψ values, and a plot of $\Delta C\alpha - \Delta C\beta$ shifts demonstrating the helical region of the coat protein subunit. This material is available free of charge via the Internet at http://pubs.acs.org.

AUTHOR INFORMATION

Corresponding Author

*E-mail: amirgo@post.tau.ac.il. Phone: 972-3-6408437. Fax: 972-3-6409293.

ACKNOWLEDGMENT

Financial support was provided by the Israel Science Foundation and a Marie-Curie reintegration grant (EU-FP7-IRG). Support for the spectrometer was given by the Center for Nanoscience and Nanotechnology of Tel Aviv University. The fth1 vector was a kind gift from Prof. Jonathan Gershoni from the Department of Cell Research and Immunology, Faculty of Life

Sciences, Tel Aviv University. The DH5α cells were a kind gift from Prof. Itai Benhar, Department of Microbiology and Biotechnology, Tel Aviv University. We thank Loren Day for general help with all aspects of the bacteriophage structure and Ivan Sergeyev for insights into the DNA structure.

REFERENCES

(1) Hoffmann-Berling, H.; Marvin, D. A.; Durwald, H. *Z. Naturforsch.* **1963**, *B 18*, 876.
(2) Lopez, J.; Webster, R. E. *Virology* **1983**, *127*, 177.
(3) Russel, M. *Mol. Microbiol.* **1991**, *5*, 1607.
(4) Marvin, D. A. *Curr. Opin. Struct. Biol.* **1998**, *8*, 150.
(5) Paschke, M. *Appl. Microbiol. Biotechnol.* **2006**, *70*, 2.
(6) Hemminga, M.; Vos, W.; Nazarov, P.; Koehorst, R.; Wolfs, C.; Spruijt, R.; Stopar, D. *Eur. Biophys. J.* **2010**, *39*, 541.
(7) Azzazy, H. M. E.; Highsmith, J. W. E. *Clin. Biochem.* **2002**, *35*, 425.
(8) Benhar, I.; Reiter, Y. *Phage Display of Single-Chain Antibody Constructs*; John Wiley & Sons: New York, 2001.
(9) Clark, J. R.; March, J. B. *Trends Biotechnol.* **2006**, *24*, 212.
(10) Huang, Y.; Chiang, C. Y.; Lee, S. K.; Gao, Y.; Hu, E. L.; Yoreo, J. D.; Belcher, A. M. *Nano Lett.* **2005**, *5*, 1429.
(11) Mao, C. B.; Solis, D. J.; Reiss, B. D.; Kottmann, S. T.; Sweeney, R. Y.; Hayhurst, A.; Georgiou, G.; Iverson, B.; Belcher, A. M. *Science* **2004**, *303*, 213.
(12) Gonzales, A.; Nave, C.; Marvin, D. A. *Acta Crystallogr., D* **1995**, *51*, 792.
(13) Thiriot, D. S.; Nevzorov, A. A.; Zagyanskiy, L.; Wu, C. H.; Opella, S. J. *J. Mol. Biol.* **2004**, *341*, 869.
(14) Straus, S.; Scott, W.; Schwieters, C.; Marvin, D. *Eur. Biophys. J.* **2011**, *40*, 221.
(15) Liu, D. J.; Day, L. A. *Science* **1994**, *265*, 671.
(16) Welsh, L. C.; Symmons, M. F.; Nave, C.; Perham, R. N.; Marseglia, E. A.; Marvin, D. A. *Macromolecules* **1996**, *29*, 7075.
(17) Tan, W. M.; Jelinek, R.; Opella, S. J.; Malik, P.; Terry, T. D.; Perham, R. N. *J. Mol. Biol.* **1999**, *286*, 787.
(18) Wang, Y. A.; Yu, X.; Overman, S.; Tsuboi, M.; Thomas, J. G. J.; Egelman, E. H. *J. Mol. Biol.* **2006**, *361*, 209.
(19) Tomar, S.; Green, M. M.; Day, L. A. *J. Am. Chem. Soc.* **2007**, *129*, 3367.
(20) Berkowitz, S. A.; Day, L. A. *J. Mol. Biol.* **1976**, *102*, 531.
(21) Marzec, C. J.; Day, L. A. *Biophys. J.* **1983**, *42*, 171.
(22) Hunter, G. J.; Rowitch, D. H.; Perham, R. N. *Nature* **1987**, *327*, 252.
(23) Barry, E.; Beller, D.; Dogic, Z. *Soft Matter* **2009**, *5*, 2563.
(24) Marvin, D. A.; Welsh, L. C.; Symmons, M. F.; Scott, W. R. P.; Straus, S. K. *J. Mol. Biol.* **2006**, *355*, 294.
(25) Zeri, A. C.; Mesleh, M. F.; Nevzorov, A. A.; Opella, S. J. *Proc. Natl. Acad. Sci. U.S.A.* **2003**, *100*, 6458.
(26) Marvin, D. A.; Hale, R. D.; Nave, C.; Citterich, M. H. *J. Mol. Biol.* **1994**, *235*, 260.
(27) Marvin, D. A.; Pigram, W. J.; Wiseman, R. L.; Wachtel, E. J.; Marvin, F. J. *J. Mol. Biol.* **1974**, *88*, 581.
(28) Caspar, D. L. D.; Makowski, L. *J. Mol. Biol.* **1981**, *145*, 611.
(29) Marvin, D. A. *J. Mol. Biol.* **1966**, *15*, 8.
(30) Day, L. A. *J. Mol. Biol.* **1966**, *15*, 395.
(31) Straus, S.; Scott, W.; Symmons, M.; Marvin, D. *Eur. Biophys. J.* **2008**, *37*, 521.
(32) Gall, C. M.; Cross, T. A.; DiVerdi, J. A.; Opella, S. J. *Proc. Natl. Acad. Sci. U.S.A.* **1982**, *79*, 101.
(33) Colnago, L. A.; Valentine, K. G.; Opella, S. J. *Biochemistry* **1987**, *26*, 847.
(34) Casadevall, A.; Day, L. A. *Biochemistry* **1983**, *22*, 4831.
(35) Cross, T. A.; Tsang, P.; Opella, S. J. *Biochemistry* **1983**, *22*, 721.
(36) Thomas, G. J.; Prescott, B.; Opella, S. J.; Day, L. A. *Biochemistry* **1988**, *27*, 4350.
(37) Aubrey, K. L.; Thomas, G. J. *Biophys. J.* **1991**, *60*, 1337.
(38) Wen, Z. Q.; Overman, S. A.; Thomas, G. J. *Biochemistry* **1997**, *36*, 7810.
(39) Day, L. A. *J. Mol. Biol.* **1969**, *39*, 265.
(40) Day, L. A.; Wiseman, R. L.; Marzec, C. J. *Nucleic Acids Res.* **1979**, *7*, 1393.
(41) Goldbourt, A.; Gross, B. J.; Day, L. A.; McDermott, A. E. *J. Am. Chem. Soc.* **2007**, *129*, 2338.
(42) Goldbourt, A.; Day, L. A.; McDermott, A. E. *J. Biol. Chem.* **2010**, *285*, 37051.
(43) Lorieau, J. L.; Day, L. A.; McDermott, A. E. *Proc. Natl. Acad. Sci. U.S.A.* **2008**, *105*, 10366.
(44) Enshell-Seijffers, D.; Smelyanski, L.; Gershoni, J. M. *Nucleic Acids Res.* **2001**, *29*, e50.
(45) Morcombe, C. R.; Zilm, K. W. *J. Magn. Reson.* **2003**, *162*, 479.
(46) McDermott, A. E.; Gu, Z. In *Encyclopedia of Nuclear Magnetic Resonance*; Grant, D. M., Harris, R., Eds.; John Wiley & Sons: New York, 1996; Vol. 2; p 1137.
(47) Takegoshi, K.; Nakamura, S.; Terao, T. *Chem. Phys. Lett.* **2001**, *344*, 631.
(48) Morcombe, C. R.; Gaponenko, V.; Byrd, R. A.; Zilm, K. W. *J. Am. Chem. Soc.* **2004**, *126*, 7196.
(49) Bennett, A. E.; Griffin, R. G.; Ok, J. H.; Vega, S. *J. Chem. Phys.* **1992**, *96*, 8624.
(50) Hong, M. *J. Biomol. NMR* **1999**, *15*, 1.
(51) Straus, S. K. *Philos. Trans. R. Soc. London, B* **2004**, *359*, 997.
(52) Bockmann, A. *C. R. Chim.* **2006**, *9*, 381.
(53) Baldus, M. *J. Biomol. NMR* **2007**, *39*, 73.
(54) Goldbourt, A. Magic-angle spinning solid state NMR: Application to structural biology. In *Encyclopedia of Analytical Chemistry*; Meyers, R. A., Ed.; John Wiley & Sons: New York, 2011; Vols. S1−S3; p 99.
(55) Sperling, L. J.; Berthold, D. A.; Sasser, T. L.; Jeisy-Scott, V.; Rienstra, C. M. *J. Mol. Biol.* **2010**, *399*, 268.
(56) Hartmann, S. R.; Hahn, E. L. *Phys. Rev.* **1962**, *128*, 2042.
(57) Stejskal, E. O.; Schaefer, J.; Waugh, J. S. *J. Magn. Reson.* **1977**, *28*, 105.
(58) Metz, G.; Wu, X. L.; Smith, S. O. *J. Magn. Reson., Ser. A* **1994**, *110*, 219.
(59) Andrew, E. B.; Chad, M. R.; Michele, A.; Lakshmi, K. V.; Robert, G. G. *J. Chem. Phys.* **1995**, *103*, 6951.
(60) Thakur, R. S.; Kurur, N. D.; Madhu, P. K. *Chem. Phys. Lett.* **2006**, *426*, 459.
(61) Schaefer, J.; McKay, R. A.; Stejskal, E. O. *J. Magn. Reson.* **1979**, *34*, 443.
(62) Baldus, M.; Geurts, D. G.; Hediger, S.; Meier, B. H. *J. Magn. Reson., A* **1996**, *118*, 140.
(63) Delaglio, F.; Grzesiek, S.; Vuister, G. W.; Zhu, G.; Pfeifer, J.; Bax, A. *J. Biomol. NMR* **1995**, *6*, 277.
(64) Goddard, T. D.; Kneller, D. G. *SPARKY*, version 3.113; University of California: San Francisco, CA, 2006.
(65) Yang, J.; Tasayco, M. L.; Polenova, T. *J. Am. Chem. Soc.* **2008**, *130*, 5798.
(66) Siemer, A. B.; McDermott, A. E. *J. Am. Chem. Soc.* **2008**, *130*, 17394.
(67) Pintacuda, G.; Giraud, Nicolas; Pierattelli, R.; Bockmann, A.; Bertini, I.; Emsley, L. *Angew. Chem., Int. Ed.* **2007**, *46*, 1079.
(68) Nadaud, P.; Helmus, J.; Jaroniec, C. *Biomol. NMR Assignments* **2007**, *1*, 117.
(69) Marulanda, D.; Tasayco, M. L.; Cataldi, M.; Arriaran, V.; Polenova, T. *J. Phys. Chem. B* **2005**, *109*, 18135.
(70) Franks, W. T.; Zhou, D. H.; Wylie, B. J.; Money, B. G.; Graesser, D. T.; Frericks, H. L.; Sahota, G.; Rienstra, C. M. *J. Am. Chem. Soc.* **2005**, *127*, 12291.
(71) Igumenova, T. I.; McDermott, A. E.; Zilm, K. W.; Martin, R. W.; Paulson, E. K.; Wand, A. J. *J. Am. Chem. Soc.* **2004**, *126*, 6720.
(72) Bockmann, A.; Lange, A.; Galinier, A.; Luca, S.; Giraud, N.; Juy, M.; Heise, H.; Montserret, R.; Penin, F. o.; Baldus, M. *J. Biomol. NMR* **2003**, *27*, 323.

(73) Pauli, J.; Baldus, M.; van Rossum, B.; Groot, H. d.; Oschkinat, H. *ChemBioChem* **2001**, *2*, 272.
(74) McDermott, A.; Polenova, T.; Bockmann, A.; Zilm, K. W.; Paulsen, E. K.; Martin, R. W.; Montelione, G. T. *J. Biomol. NMR* **2000**, *16*, 209.
(75) Shi, L.; Kawamura, I.; Jung, K.-H.; Brown, L. S.; Ladizhansky, V. *Angew. Chem.* **2011**, *123*, 1338.
(76) Jehle, S.; van Rossum, B.; Stout, J. R.; Noguchi, S. M.; Falber, K.; Rehbein, K.; Oschkinat, H.; Klevit, R. E.; Rajagopal, P. *J. Mol. Biol.* **2009**, *385*, 1481.
(77) Li, Y.; Berthold, D. A.; Gennis, R. B.; Rienstra, C. M. *Protein Sci.* **2008**, *17*, 199.
(78) Huang, L.; McDermott, A. E. *Biochim. Biophys. Acta, Bioenergetics* **2008**, *1777*, 1098.
(79) van Gammeren, A. J.; Hulsbergen, F. B.; Hollander, J. G.; de Groot, H. J. M. *J. Biomol. NMR* **2005**, *31*, 279.
(80) Helmus, J. J.; Surewicz, K.; Nadaud, P. S.; Surewicz, W. K.; Jaroniec, C. P. *Proc. Natl. Acad. Sci. U.S.A.* **2008**, *105*, 6284.
(81) Heise, H.; Celej, M. S.; Becker, S.; Riede, D.; Pelah, A.; Kumar, A.; Jovin, T. M.; Baldus, M. *J. Mol. Biol.* **2008**, *380*, 444.
(82) Zhou, D. H.; Woods, W. S.; Kloepper, K. D.; Ladror, D.; Hartman, K.; George, J. M.; Rienstra, C. M. *Biophys. J.* **2007**, 149A.
(83) Van der Wel, P. C. A.; Lewandowski, J. R.; Griffin, R. G. *J. Am. Chem. Soc.* **2007**, *129*, 5117.
(84) Heise, H.; Hoyer, W.; Becker, S.; Andronesi, O. C.; Riedel, D.; Baldus, M. *Proc. Natl. Acad. Sci. U.S.A.* **2005**, *102*, 15871.
(85) Day, L. A.; Hendrix, R. W. Inoviridae. In *Virus Taxonomy: Eighth Report of the International Committee on the Taxonomy of Viruses*; Fauquet, C. M., Mayo, M. A., Maniloff, J., Desselberger, U., Ball, L. A., Eds.; Elsevier: Amsterdam, The Netherlands, 2005; p 277.
(86) Spera, S.; Bax, A. *J. Am. Chem. Soc.* **1991**, *113*, 5490.
(87) Wang, Y. J.; Jardetzky, O. *Protein Sci.* **2002**, *11*, 852.
(88) Arnold, G. E.; Day, L. A.; Dunker, A. K. *Biochemistry* **1992**, *31*, 7948.
(89) Takeuchi, H.; Matsuno, M.; Overman, S. A.; Thomas, G. J. *J. Am. Chem. Soc.* **1996**, *118*, 3498.
(90) Matsuno, M.; Takeuchi, H.; Overman, S. A.; Thomas, G. J., Jr. *Biophys. J.* **1998**, *74*, 3217.
(91) Santos, R. A.; Tang, P.; Harbison, G. S. *Biochemistry* **1989**, *28*, 9372.
(92) Loquet, A.; Lv, G.; Giller, K.; Becker, S.; Lange, A. *J. Am. Chem. Soc.* **2011**, *133*, 4722.
(93) Shen, Y.; Delaglio, F.; Cornilescu, G.; Bax, A. *J. Biomol. NMR* **2009**, *44*, 213.
(94) Berjanskii, M. V.; Neal, S.; Wishart, D. S. *Nucleic Acids Res.* **2006**, *34*, W63.
(95) Luca, S.; Filippov, D. V.; van Boom, J. H.; Oschkinat, H.; de Groot, H. J. M.; Baldus, M. *J. Biomol. NMR* **2001**, *20*, 325.
(96) Weiss, M. S.; Jabs, A.; Hilgenfeld, R. *Nat. Struct. Mol. Biol.* **1998**, *5*, 676.
(97) Schubert, M.; Labudde, D.; Oschkinat, H.; Schmieder, P. *J. Biomol. NMR* **2002**, *24*, 149.
(98) Voet, D.; Voet, J. G. *Biochemistry*, 2nd ed.; Wiley: New York, 1995.
(99) Kabsch, W.; Sander, C. *Biopolymers* **1983**, *22*, 2577.
(100) Day, L. A.; Marzec, C. J.; Reisberg, S. A.; Casadevall, A. *Annu. Rev. Biophys. Biophys. Chem.* **1988**, *17*, 509.
(101) Ebrahimi, M.; Rossi, P.; Rogers, C.; Harbison, G. S. *J. Magn. Reson.* **2001**, *150*, 1.
(102) Xu, X.-P.; Chiu, W.-L. A. K.; Au-Yeung, S. C. F. *J. Am. Chem. Soc.* **1998**, *120*, 4230.
(103) Dejaegere, A. P.; Case, D. A. *J. Phys. Chem. A* **1998**, *102*, 5280.
(104) Sergeyev, I.; Goldbourt, A.; Day, L. A.; McDermott, A. E. Chemical shifts for the unusual DNA structure in Pf1 bacteriophage from dynamic-nuclear-polarization-enhanced solid-state NMR spectroscopy. *J. Am. Chem. Soc.*, submitted.
(105) Tsuboi, M.; Tsunoda, M.; Overman, S. A.; Benevides, J. M.; Thomas, G. J. *Biochemistry* **2010**, *49*, 1737.
(106) Ulrich, E. L.; Akutsu, H.; Doreleijers, J. F.; Harano, Y.; Ioannidis, Y. E.; Lin, J.; Livny, M.; Mading, S.; Maziuk, D.; Miller, Z.; Nakatani, E.; Schulte, C. F.; Tolmie, D. E.; Kent Wenger, R.; Yao, H.; Markley, J. L. *Nucleic Acids Res.* **2008**, *36*, D402.
(107) Shen, Y.; Lange, O.; Delaglio, F.; Rossi, P.; Aramini, J. M.; Liu, G.; Eletsky, A.; Wu, Y.; Singarapu, K. K.; Lemak, A.; Ignatchenko, A.; Arrowsmith, C. H.; Szyperski, T.; Montelione, G. T.; Baker, D.; Bax, A. *Proc. Natl. Acad. Sci. U.S.A.* **2008**, *105*, 4685.
(108) Cavalli, A.; Salvatella, X.; Dobson, C. M.; Vendruscolo, M. *Proc. Natl. Acad. Sci. U.S.A.* **2007**, *104*, 9615.